A time-domain model for railway rolling noise

Jannik Theyssen, Astrid Pieringer, Wolfgang Kropp
Division of Applied Acoustics, Chalmers University of Technology, 41258 Gothenburg, Sweden
Email: jannik.theyssen@chalmers.se

Introduction

Transport is one of the main drivers for human-made climate change. Increasing the share of railway traffic can contribute to lower carbon emissions from the transport sector. This will, however, lead to increased noise emissions from railway traffic. A main contributor to these noise emissions is rolling noise, which is produced by the interaction between the wheels and the track, which vibrate when the wheels roll over the rails because their contact surfaces are not perfectly smooth. A modular simulation tool can be used to efficiently optimise track designs regarding their acoustic performance. A time-domain model further allows investigating the psychoacoustic effects of features in the noise signals.

A model that aims for a physics-based simulation of the pass-by signals has been developed in a recent doctoral project at Chalmers University of Technology [1], building on earlier work [2]. This article summarises the model. Its modular setup is visualised in Figure 1. In

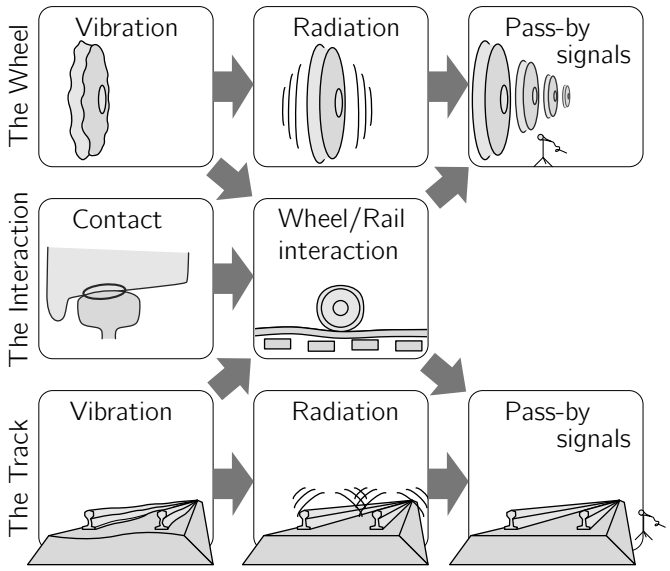

Figure 1: Overview of the modules in the simulation tool.

terms of the computational efficiency, it is advantageous to evaluate parts that can be linearised in the frequency domain. This is the case for the structural vibration and the sound radiation of the wheel and the track. Relevant non-linear behaviour can occur in the rolling contact and the wheel/rail interaction, and so these parts are evaluated in the time domain. The latter modules were developed in [2]. For the wheel and the track, transfer functions are evaluated that describe the sound pressure in a receiver point for a unit force excitation. An inverse Fourier transform then produces impulse responses, which are convolved with the force signal calculated in the wheel/rail interaction calculation. Each component is described in the following.

The Interaction

The interaction between the wheel and the track needs two models, one for solving the contact problem and one for solving the wheel/rail interaction [2].

The Contact

The contact model combines the information about the surface roughness of the wheel and the rail with the local geometry to predict the shape and size of the contact area, local displacements and stresses. The input roughnesses can be measured or generated based on statistical properties of the surface roughness. Figure 2 shows examples of such surface roughness input data. Wheel and

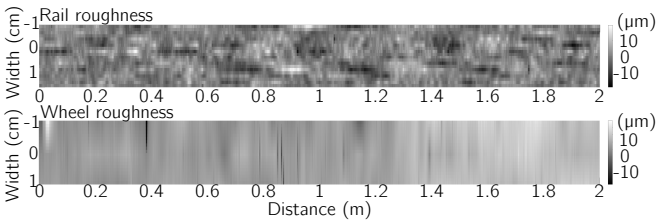

Figure 2: Example input data for the contact problem.

rail are locally approximated by an elastic half space. The potential contact area is discretised into rectangular elements. Each element influences each other element and a non-linear system of equations needs to be solved at each time step. Kalker's NORM and TANG algorithm are used to solve the normal and tangential problem, respectively [3]. The normal and tangential local displacements in the contact patch at each time-step are, input to the wheel/rail interaction calculation.

The Wheel/Rail Interaction

The wheel/rail interaction is efficiently solved in the time domain via moving Green's functions [3]. The Green's functions are precalculated and contain the dynamic properties of the wheel, specifically the displacement impulse response functions at the contact point, and the dynamic properties of the track, i.e. the displacement impulse response functions at the contact point on the rail. Combining this with the local displacements in the contact patch at every time step, the rolling contact forces are calculated by convolution. This time-domain formulation allows including transient and non-linear effects such as wheel flats and curve squeal. Figure 3 shows an example time history of rolling contact forces.

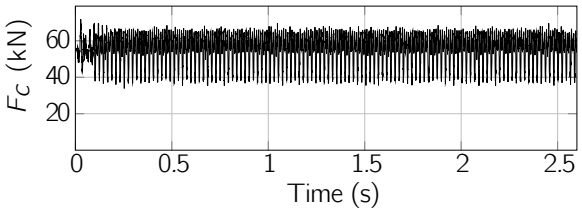

Figure 3: Example rolling contact forces.

The Wheel

Structural Vibration

The curved Waveguide Finite Element (WFE) method assumes harmonic oscillation around the circumference of the wheel [4]. Similar to axi-symmetric FE models, the 3D vibration of the wheel is calculated by discretising the cross-section only, cf. Figure 4. The FE system of

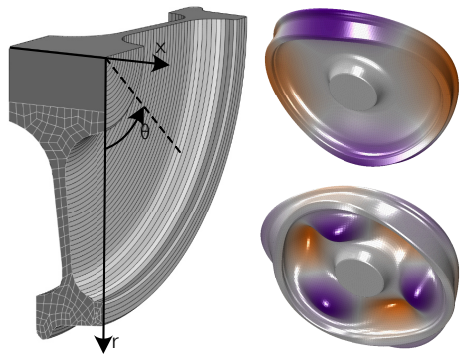

Figure 4: Left: Wheel FE grid and coordinate system. Upper right: Axial mode with two nodal diameters. Lower right: axial mode with three nodal diameters and one nodal circle.

equations

$$\left[\mathbf{K}_2(-j\kappa)^2 + \mathbf{K}_1(-j\kappa) + \mathbf{K}_0 - \omega^2\mathbf{M}\right]\mathbf{\Phi} = 0 \qquad (1)$$

is solved for each whole number wavenumber κ corresponding to the number of oscillations around the circumference. This produces the eigenfrequencies ω_0 and mode shapes $\mathbf{\Phi}_l$ of the wheel. $\mathbf{K}$ and $\mathbf{M}$ are stiffness- and mass matrices. The velocity field $\mathbf{v}$ on the wheel due to a force $\mathbf{F}_e(\omega)$ is obtained by modal superposition,

$$\mathbf{v}(\omega) = \sum_l A_l(\omega)\mathbf{\Phi}_l \qquad (2)$$

with the modal amplitude A_l

$$A_l(\omega) = j\omega b_l(\omega)\mathbf{F}_e(\omega)\mathbf{\Phi}_l(\mathbf{x}_0) \qquad (3)$$

where

$$b_l(\omega) = \left(\Lambda_l(\omega_l^2 - \omega^2 + 2j\omega\omega_l\zeta_l)\right)^{-1} \qquad (4)$$

with the modal damping coefficient ζ_l and the modal mass

$$\Lambda_l = \mathbf{\Phi}_l^{\mathrm{H}}\mathbf{M}\mathbf{\Phi}_l \ . \qquad (5)$$

The velocity field serves as the input to the sound radiation module. Analogously, the receptance at the rolling contact point on the wheel is evaluated. The displacement impulse response functions are calculated by inverse Fourier transform and serve as input to the wheel/rail interaction module.

Sound Radiation

The sound radiated by each wheel mode is evaluated in a Fourier series Boundary Element method (FBEM), which makes use of the axisymmetry of the wheel by decomposing the sound field into a Fourier series [4]. The BE problem reduces from 3D to 2D, however, now 2D BE problems are solved at each Fourier order. While FBEM is an efficient solution for predicting the sound field around a vibrating, stationary wheel, it is not convenient for simulating the pass-by of a wheel in time domain. Therefore an equivalent source model is introduced for this part.

Representing the sound field by spherical harmonics (SH) equivalent sources allows the efficient calculation of sound pressure transfer functions $H_l(x_s, y_0, z_0, \omega)$ to any receiver position in 3D space. To calculate these transfer functions, first the FBEM is used to evaluate the sound field in a spherical grid around the wheel for each mode l at each frequency. Then, SH decompositions are carried out for each such sound field. Figure 5 shows the directivity of the axial mode (3,1,a) for two different frequencies. The radius of the lobes indicates the magnitude of the radiation, while the colour indicates the phase. At the higher frequency, the radiation is more directed and larger phase variation is visible. Note also that this axial mode has large radial components at 250 Hz.

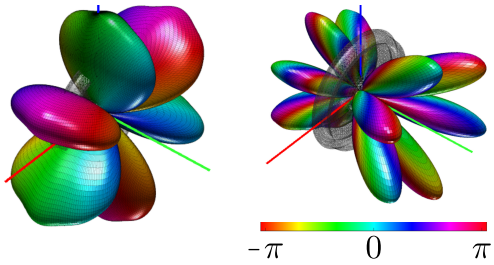

Figure 5: Directivity of the mode (3,1,a) shown in Figure 4 at 250 Hz (left) and 1000 Hz (right). The red line indicates the track direction.

Pass-by Signals

The sound pressure produced when one wheel passes by a stationary observer position is evaluated for each mode individually [1]. This has computational advantages: Since the wheel is typically only very lightly damped, it can have decay times of over 20 seconds. Calculating Green's functions that include the structural response is therefore not feasible in the proposed BEM/SH method. By following a modal approach in the pass-by prediction, the structural response can be separated from the acoustic radiation: The modal amplitude $A_l(\omega)$ consists of the two terms $A_l(\omega) = F_{A,l}b_l(\omega)$. $F_{A,l}(\omega)$ is expressed in time domain by differentiating $\mathbf{F}_e(\omega)$ and scaling with $\mathbf{\Phi}_l$. The term $b_l(v\omega)$ describes the frequency response of an harmonic oscillator, for which an analytic expression exists:

$$b_l = \frac{\mathrm{e}^{=2\omega_l\zeta_l t}}{\Lambda_l\omega_l'}\sin\omega_l' t\mathrm{H}(t) \qquad (6)$$

with the Heaviside function $\mathrm{H}(t)$.

The coordinates of the moving wheel and the stationary receiver are introduced in Figure 6. Convolution of $b_l(t)$

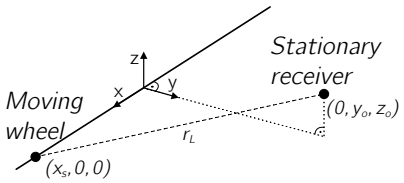

Figure 6: Coordinates of the moving wheel and the stationary receiver.

and $F_{A,l}(x_s, t)$ produces a quantity $q'_{\mathrm{S},l}$

$$q'_{\mathrm{S},l}(x_\mathrm{S}, x_\mathrm{S}/v) = \int_{-\infty}^{x_\mathrm{S}/v} F_{A,l}(x_\mathrm{S}, \tau) b_l(x_\mathrm{S}/v - \tau) \mathrm{d}\tau \quad (7)$$

which describes the amplification of each mode at each time step, taking into account the history of all contact forces and the dynamic response of the mode. Then, acoustic propagation functions $h_l(x_\mathrm{S}, t)$ are evaluated by inverse Fourier transform for each mode, and finally, convolution of $q'_{\mathrm{S},1}$ and h_l produces the pass-by pressure of mode l

$$p_l(t) = \int_{-\infty}^{\infty} q'_{\mathrm{S},l}(x_\mathrm{S}, x_\mathrm{S}/v) h_l(x_\mathrm{S}, t - x_\mathrm{S}/v) \mathrm{d}x_\mathrm{S} \quad (8)$$

The computational advantage of this modal approach is that the acoustic propagation functions $H_l(\omega)$ are rather smooth, so they can be evaluated with a broad frequency spacing.

The total pressure is then calculated as the sum of all modal contributions. Figure 7 shows a spectrogram of

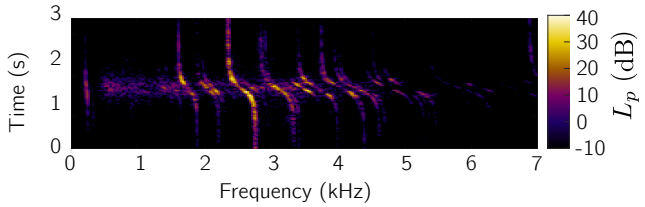

Figure 7: Spectrogram of the sound pressure level during pass-by of wheel.

the sound pressure in a stationary point during the pass-by of the wheel. The Doppler shift is clearly visible, and a few dominant modes can be identified. The largest sound pressure levels are produced in the frequency range between about 1.7 kHz and 4.5 kHz.

The Track Structural Vibration

The WFE method can also be used for straight waveguides such as the rail [5, 1]. Making use of the constant cross-section along the track and assuming propagating, decaying waves in that dimension, the FE problem is again reduced to 2D (cf. Figure 8). However, in this straight case, complex wavenumbers exists at each frequency ω. Prescribing ω, the quadratic FE system of equations

$$\left[\mathbf{K}_2(-j\kappa)^2 + \mathbf{K}_1(-j\kappa) + \mathbf{K}_0 - \omega^2\mathbf{M}\right]\mathbf{\Phi} = 0 \quad (9)$$

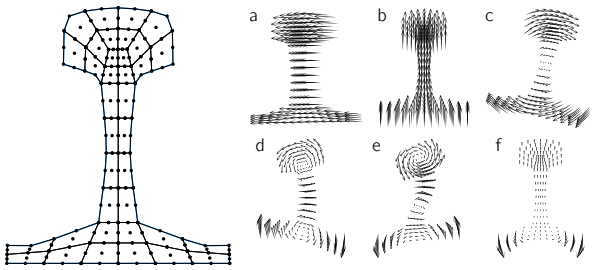

Figure 8: Left: FE mesh of the free rail cross-section. Right: Cross-sectional modes for wavenumber 5 rad/m.

is solved. This produces conjugate complex wavenumbers κ_i and corresponding eigenvectors $\mathbf{\Phi}_l$, which describe the cross-sectional motion of each wave (cf. Figure 8). The displacement response $\mathbf{u}(x, \omega)$ to the force $\mathbf{F}_0(\kappa, \omega)$ is calculated by superposition of all waves,

$$\mathbf{u}(x, \omega) = \sum_i A_i \Phi_{i,R} \mathrm{e}^{-j\kappa_i x} \text{ for } \geq 0 \quad (10)$$

with

$$A_i = \frac{j\mathbf{\Phi}_{iL}\mathbf{F}_0(\kappa, \omega)}{\mathbf{\Phi}_{iL}\mathbf{D}(\kappa_i)\mathbf{\Phi}_{iR}} \quad (11)$$

and $\mathbf{D}(\kappa_i) = -2\kappa_i\mathbf{K}_2 - j\mathbf{K}_1$.

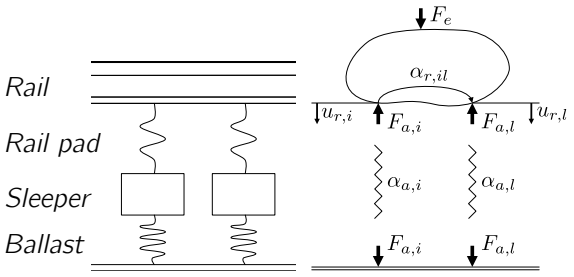

Figure 9: Components in the discrete support of the rail.

In reality, the rail is coupled to the rest of the track at each rail seat via the elastic rail pad, cf. Figure 9. A discrete support is introduced by assuming that the displacement response of the coupled system is a superposition of the free rail response and the response due to the reaction forces,

$$u_{r,i} = \alpha_{r,ie}F_e - \sum_{l=1}^{N} \alpha_{r,il}F_{a,l} \quad (12)$$

where the transfer receptances α_r are evaluated using the WFE model above. Modelling each rail seat receptance α_a as lumped elements produces one equation $u_{r,i} = \alpha_{a,i}F_{a,i}$ for each rail seat. A system of equations is set up and solved for the unknown reaction forces $\mathbf{F}_a$. The total displacement of the rail is then calculated by summing the displacements due to each force acting on the rail. Figure 10 shows the vertical velocity of one FE node at the top of the rail head, for a vertical unit harmonic excitation of the rail mid-span, in the wavenumber and frequency domain. Up to about 4 kHz, the vertical bending wave dominates the response. At higher frequencies, other wave types cut in.

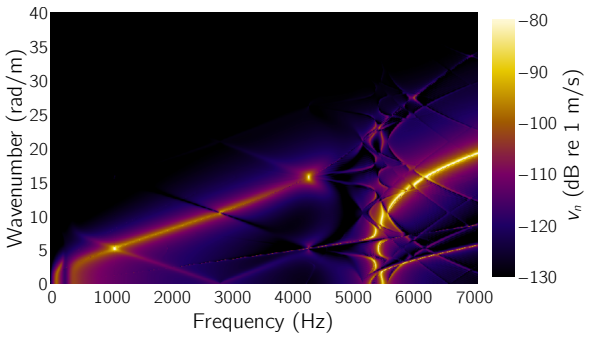

Figure 10: Surface normal velocity of the rail head in the frequency-wavenumber domain.

Sound Radiation

The radiation from railway track is calculated using the Wavenumber domain Boundary Element method (WBEM), which assumes a constant cross-section along the track [6]. In the WBEM, the 3D sound field (with the wavenumber in air K) is expressed as 2D sound fields (with in-plane wavenumber α) at each wavenumber κ along the track. The reduction in dimensionality in the BE problem reduces the computational cost. To further increase the numerical efficiency, acoustic transfer functions $H_a(\kappa, \omega)$ are precalculated. These describe the sound pressure produced at a set of receiver positions for a unit velocity at each BE node. This allows the total radiated sound pressure from a vibrating structure to be evaluated by scaling each transfer function with the surface velocity at the corresponding node and summing their contributions. A second way to increase the numerical efficiency is to reuse 2D BE solutions across different combinations of wavenumber κ [6, 1].

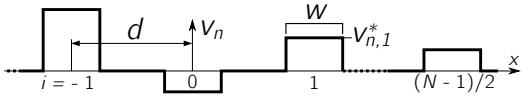

Figure 11: Velocity profile of several sleepers along the track direction x.

The radiation from each sleeper is included in the WBEM by introducing a velocity profile $v_{n,i}$ (cf. Figure 11). Each velocity profile is expressed as a rectangular function defined by the position id and the width w of the sleeper, scaled to the sleeper's vertical velocity $v^*_{n,i}$

$$v_{n,i}(x,\omega) = v^*_{n,i}(\omega)\left(\mathrm{H}\left(x - id + \frac{w}{2}\right) - \mathrm{H}\left(x - id - \frac{w}{2}\right)\right) \tag{13}$$

which are expressed in wavenumber domain as $v_{n,i}(\kappa,\omega) = v^*_{n,i}\, w\, \mathrm{sinc}(\kappa w)\mathrm{e}^{-j\kappa id}$ and serves as the input to the WBEM calculation.

Pass-by Signals

Multiplying the velocity of one surface element for a unit harmonic force input (cf. Figure 10) with its corresponding transfer function $H_a(\kappa, \omega)$, and subsequent 2D inverse Fourier transform generates impulse responses describing the pressure response to a unit force pulse. Convolution of these impulse responses with a rolling contact force allows calculating the sound pressure in a stationary track-side position. An example pass-by on the rail is visualised in the spectrogram in Figure 12. The largest levels are observed in the frequency range below 1 kHz, however, some tonal components are visible at higher frequencies, likely due to the structural interaction between the components.

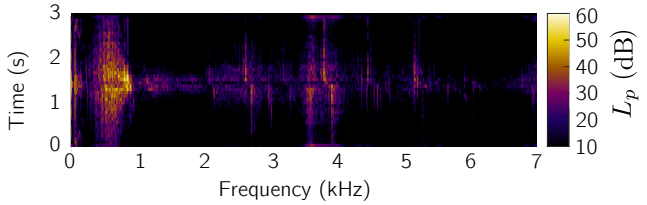

Figure 12: Spectrogram of the sound pressure level during pass-by of a force on the rail.

Summary

This article gives a brief overview of the time-domain rolling noise model WERAN developed in two PhD projects at Chalmers University [1, 2]. The interaction between the wheel and the rail, their vibroacoustic behaviour and the sound pressure level during the pass-by of a wheel on a rail are evaluated in a modular approach incorporating various numerical models.

Acknowledgements

The current study is part of the ongoing activities in CHARMEC (Chalmers Railway Mechanics). Parts of the study have been funded from the European Union's Horizon 2020 research and innovation programme in the In2Track3 project under grant agreements No 101012456.

References

[1] Theyssen J. Simulating Rolling Noise on Ballasted and Slab Tracks: Vibration, Radiation, and Pass-by Signals. Doctoral Thesis. Chalmers University of Technology; 2022.

[2] Pieringer A. Time-Domain Modelling of High-Frequency Wheel/Rail Interaction. Doctoral Thesis. Chalmers University of Technology; 2011.

[3] Pieringer A, Kropp W, Thompson DJ. Investigation of the dynamic contact filter effect in vertical wheel/rail interaction using a 2D and a 3D non-Hertzian contact model. Wear. 2011;271(1):328-338.

[4] Fabre F, Theyssen JS, Pieringer A, Kropp W. Sound radiation from railway wheels including ground reflections: A half-space formulation for the fourier boundary element method. JSV. 2021;493:115822.

[5] Nilsson CM, Jones CJC, Thompson DJ, Ryue J. A waveguide finite element and boundary element approach to calculating the sound radiated by railway and tram rails. JSV. 2009;321(3-5):813-836.

[6] Theyssen J, Pieringer A, Kropp W. Efficient calculation of the three-dimensional sound pressure field around a railway track. Published online 2022. Accessed June 28, 2022. https://research.chalmers.se/en/publication/530940